Radially Polarized Light for Detection and Nanolocalization of Dielectric Particles on a Planar Substrate

S. Roy,* K. Ushakova, Q. van den Berg, S. F. Pereira, and H. P. Urbach
Department of Imaging Physics, Delft University of Technology, Lorentzweg 1, 2628 CJ Delft, Netherlands
(Received 8 December 2014; published 12 March 2015)

A fast noninvasive method based on scattering from a focused radially polarized light to detect and localize subwavelength nanoparticles on a substrate is presented. The technique relies on polarization matching in the far field between scattered and spurious reflected fields. Results show a localization uncertainty of $\approx 10^{-4}\lambda^2$ is possible for a particle of area $\approx\lambda^2/16$. The effect of simple pupil shaping is also shown.

DOI: 10.1103/PhysRevLett.114.103903 PACS numbers: 42.25.Fx, 42.25.Ja, 42.30.Kq

Nanoparticle detection is an issue in many branches of science, and several ways to solve this problem have been studied. The problem can be classified into two main categories: particles in a solution, having importance in the field of biological microscopy [1,2], and particles on a substrate. This second type is especially encountered in contamination issues, for example, in lithography, nanofabrication, and surface science, in general. However, there are often situations where an object of a size below the optical diffraction limit must be sensed but the high resolution imaging solutions, like scanning electron microscope or superresolution techniques [3], are not of practical use. An important example is the high volume production of organic electronic devices, which, in present days, are migrating from a sheet-to-sheet to a roll-to-roll production line [4]. A critical criterion here is to quantify the contamination of the substrate by estimating the number of particles and defects on it before actual fabrication. The typical sizes of contaminating particles or defects range from tens of nanometers to a few microns. The inspection must be performed in line, thereby implying speed to be a very important parameter (typical speeds are a few hundreds of centimeters per second [5]). Additionally, it is also desired to locate the positions of contaminating particles or defects, especially those in some critical locations of the substrate which can create serious issues for further fabrication [6,7]. The final goal, detection or detection localization (slower), determines the inspection speed. Scanning-based scattering techniques for particle detection are ideal for these situations. However, they still suffer from their complexity and lack of speed, since most of them utilize multiple beams and detectors and rely on correlations between them [8]. Moreover, in most cases the desired detection sensitivity is achieved only by using wavelengths shorter than Ultraviolet B (280–315 nm) [8] or high power [9], either of which are often harmful for organic substrates [10].

In this Letter, we present a scattering technique which uses a simple and robust configuration and utilizes radially polarized light at $\lambda = 405$ nm to simultaneously detect subwavelength nanoparticles and locate them with high accuracy and speed, limited by experimental noise. The method is based on the interaction of the scattering and spurious reflected field and uses differential data processing, so that only differential detectors can be used for the whole detection scheme. From previous works on nanoparticle detection, it is well known that the scattered field amplitude increases with the third power of the scattering particle size and hence the intensity varies with the sixth power, implying that the field-detection-type solutions (mainly interferometric techniques) are significantly more sensitive for this problem [11]. The problem is favorable when the scattering particle is on a substrate, since then a common path interferometric phenomenon is always initiated between the reflected and scattered field which can be modulated by small shifts of the scatterer, resulting in a detectable asymmetry in the far field. This asymmetry effect is somewhat similar to the optical spin-Hall effect [12] of fields with spin momentum, although the physical principles are different.

To understand the principle in more detail, let us consider a Cartesian system (x, y, z) with z as the propagation direction. An electric dipole in air with dipole vector $\mathbf{q} = (q_x, q_y, q_z)$ at the origin radiates electric field $\mathbf{E}^{\mathrm{dip}}$ [13]:

$$\mathbf{E}^{\mathrm{dip}}(\mathbf{r}) = -\frac{k^2}{\epsilon_0}\mathbf{q}G(\mathbf{r}) - \nabla\left[\nabla.\frac{\mathbf{q}}{\epsilon_0}G(\mathbf{r})\right], \qquad (1)$$

where $G(\mathbf{r})$ is the free space Green's function and k is the wave number. Taking the Fourier transform in a plane orthogonal to z,

$$\widehat{\mathbf{E}^{\mathrm{dip}}}(k_x, k_y, z) = -[k^2\mathbf{q} - (\mathbf{k}.\mathbf{q})\mathbf{k}]\frac{e^{ik_z z}}{2ik_z}, \qquad (2)$$

where $\mathbf{k} = k_x\mathbf{x} + k_y\mathbf{y} + k_z\mathbf{z}$ is the wave vector.

The plane wave expansion of an electric field is commonly written in terms of the complex amplitudes of the perpendicular (s) and parallel (p) components to the plane of incidence [14]:

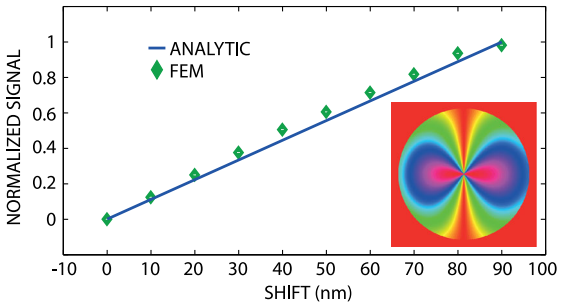

FIG. 1 (color online). A comparison between the single dipole model (blue line) and FEM simulations (green diamond) of the difference of the total intensities in the left and right halves of the pupil for the x component of the far field. FEM simulations are for a particle of diameter 100 nm on a silicon substrate ($\lambda = 405$ nm, NA $= 0.9$, substrate refractive index $5.42 + 0.33i$, and particle refractive index 1.5). In the FEM model [18], a radially polarized beam is focused at the interface with the NA divided into 10^4 incident angles. The computational domain was chosen such that the first zero of the focused electric field components fits completely in it. For $x < 100$ nm, the variation is almost linear with a slope of $1.1\%/\text{nm}$ of maximum signal, which is approximately proportional to $r_p(1 + r_p)\alpha$, for given NA, λ, and $\mathbf{A}^{\text{inc}}$. Deviation starts to build up after $x = 90$ nm as the transverse components become stronger (this area, $0.16\lambda^2$, which is slightly less than the longitudinal spot size $0.2\lambda^2$ [16], is where our model remains valid). Inset: x-polarized field $|E_x^{\text{pupil}}|$ at the pupil. For a large shift of 100 nm, visible asymmetry is observed.

$$A_s^{\text{dip}} = \frac{1}{2i\epsilon_0}\frac{k/k_z}{\sqrt{k_x^2 + k_y^2}}[kk_x q_y - kk_y q_x],$$
$$A_p^{\text{dip}} = \frac{1}{2i\epsilon_0}\frac{k/k_z}{\sqrt{k_x^2 + k_y^2}}[k_x k_z q_x + k_y k_z q_y - (k_x^2 + k_y^2) q_z], \tag{3}$$

where $\mathbf{A}^{\text{dip}} = A_s^{\text{dip}}\mathbf{s} + A_p^{\text{dip}}\mathbf{p}$ is the complex vector amplitude of the plane waves. With the proper sign of k_z, Eq. (3) is valid when the field propagates along positive or negative z. If an objective, with the z axis as the optical axis, is placed such that its geometrical focus is at the origin, then the outgoing s and p fields are, respectively, converted to an azimuthally (A_ϕ) and a radially (A_ρ) polarized field in the pupil plane through $(A_\phi^{\text{dip}}, A_\rho^{\text{dip}}) = \sqrt{k/k_z}(A_s^{\text{dip}}, A_p^{\text{dip}})$ [15]. If the dipole is on a substrate, there will be other fields besides $\mathbf{E}^{\text{dip}}$, which we are going to consider.

From Eq. (3), we note that if the dipole moment is oriented along z, i.e., $q_x = q_y = 0$, then the electric field at the pupil of the objective is purely radially polarized. Conversely, it is well known that the field at the focus of a radially polarized pupil distribution has a large longitudinal component [16,17]. Thus, a dipole, which is excited by a tightly focused radially polarized wave, will radiate radially polarized light. If the dipole is on a substrate, there will also be the spurious reflected field which is obviously radially polarized. The whole objective-dipole system works as a common path interferometer. The contrast of the superposition of this scattered field and the spurious reflected field will be high, since the interfering fields are parallel polarized at every point in the pupil. This situation arises when a subwavelength nanoparticle present on a planar surface is illuminated by a focused radially polarized wave. A reasonable approximation of the dipole moment $\mathbf{q}$ is to assume it to be proportional to the incident local electric field $\mathbf{E}^f$ at the position of the nanoparticle through the complex polarizability α which depends on the material and shape of the particle [11]. $\mathbf{E}^f$ is expressed in terms of incident plane wave amplitudes $\mathbf{A}^{\text{inc}}$ at the objective pupil as $\mathbf{E}^f(\mathbf{r}) = \int (A_\phi^{\text{inc}}\mathbf{s} + A_\rho^{\text{inc}}\mathbf{p}) e^{i\mathbf{k}\cdot\mathbf{r}}\sqrt{k_z/k}\,dk_x dk_y$.

Assuming the incident field is radially polarized before the objective, $A_s^{\text{inc}} = A_\phi^{\text{inc}}\sqrt{k_z/k} = 0$, and close to focus, $\mathbf{E}^f(\mathbf{r}) \approx E^f(\mathbf{r})\hat{z}$. Following the shift properties of the Fourier transform, if we shift the nanoparticle in the focal plane along the x axis by $r = x$, then there will be a corresponding phase shift of $ik_x x$ in the scattered far field. The resulting scattered field components can now be written from Eq. (3) as $A_s^{\text{dip}} = 0$ and

$$A_p^{\text{dip}} \approx -\frac{\alpha}{2i\epsilon_0}\left[\frac{k\sqrt{k_x^2 + k_y^2}}{k_z}\right] E^f(x) e^{ik_x x}$$
$$\approx -\frac{\alpha}{2i\epsilon_0}\left[\frac{k\sqrt{k_x^2 + k_y^2}}{k_z}\right] E^f(0) e^{ik_x x}, \tag{4}$$

where, we assume that $x \ll \lambda$.

However, there will be another part of the scattered field which is reflected from the substrate (see Fig. 2, inset). We also assume the dipole to be very close to the substrate interface so that the phase difference between the directly scattered and reflected scattered signals is very small compared to the wavelength of illumination. This assumption is approximately valid in the experiments when the beam is focused at the interface, so that the effective dipole remains very close to the surface. Moreover, this phase is not a function of x. Under this assumption, the total scattered signal can be obtained by multiplying Eq. (4) by $1 + r_p$, where r_p is the complex Fresnel reflection coefficient for p polarization. Thus, the total outgoing complex field $\mathbf{A}^{\text{out}}$ can be written as a superposition of the total scattered and spurious reflected wave as

$$A_s^{\text{out}} \approx 0 \text{ and}$$
$$A_p^{\text{out}} \approx r_p A_p^{\text{inc}} - (1 + r_p)\frac{\alpha}{2i\epsilon_0}\left[\frac{k\sqrt{k_x^2 + k_y^2}}{k_z}\right] E^f(0) e^{ik_x x}. \tag{5}$$

Here, the spurious reflected field is the incident field $\mathbf{A}^{\text{inc}}$ directly modulated by r_p. The effect of the modulation by

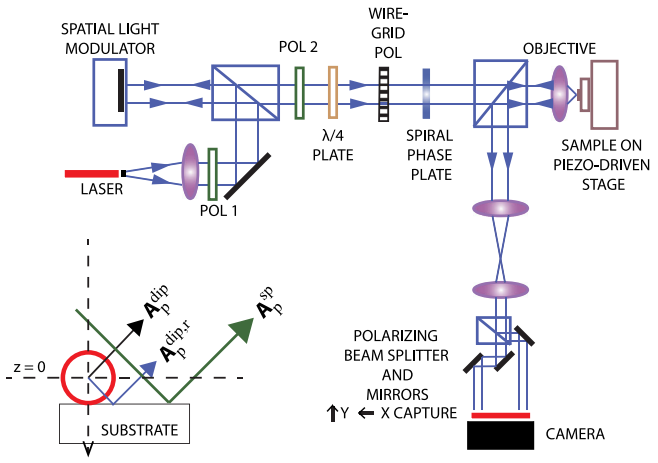

FIG. 2 (color online). Experimental schematics. The modeling of the problem is illustrated in the inset. The scattered field consists of directly scattered ($\mathbf{A}_p^{\mathrm{dip}}$) and reflected scattered ($\mathbf{A}_p^{\mathrm{dip},r}$), where, from our assumption, $\mathbf{A}_p^{\mathrm{dip},r} = r_p \mathbf{A}_p^{\mathrm{dip}}$. The specular reflected field is $\mathbf{A}_p^{\mathrm{sp}} = r_p A_p^{\mathrm{inc}} \mathbf{p}$. Thus, for each $\mathbf{k}$, the total outgoing signal is $\mathbf{A}_p^{\mathrm{out}} = \mathbf{A}_p^{\mathrm{sp}} + \mathbf{A}_p^{\mathrm{dip}} + \mathbf{A}_p^{\mathrm{dip},r}$.

shift x in the pupil is an asymmetry of energy distribution between the left and right halves. Thus, a differential analysis between these halves of the pupil will be related to the shift of the particle (a through-focus shift will also create a phase difference between the scattered signals, which is not possible for a particle on a substrate, however, that does not break the symmetry). Conveniently, no power flows on the optical axis in the pupil. This makes the system more robust for a differential analysis than incident fields without a singularity, such as the circularly polarized field. Note that the differential signal will be zero not only when there is no particle ($\mathbf{A}_p^{\mathrm{dip}} = \mathbf{0}$) but also when the particle center coincides with the spot ($x = 0$) axis restoring the symmetry. This fact can be used to localize the particle. A comparison of this analytic model with FEM simulation is shown in Fig. 1, where the differential signal between two halves of the pupil is plotted as a function of shift x.

For experimental demonstration, a sample is made by depositing polystyrene latex spheres of diameter 95 ± 7 nm on a polished silicon wafer with rms roughness < 3 nm over an area of 5 μm^2 [19]. The experimental setup is shown in Fig. 2. A collimated diode laser beam at $\lambda = 405$ nm with a beam diameter of 3.8 mm passes through two Glan-Laser prism polarizers and a Holoeye LC-R2500 spatial light modulator (SLM). The SLM is used to create an annular incident field. After that, a $\lambda/4$ plate, a wire grid polarizer, and a spiral phase plate are used to create radial polarization [20,21]. The wire grid polarizer, consisting of concentric Al cylinders on the glass substrate, was specially fabricated to generate radially polarized light at a wavelength of 405 nm. This beam is focused by an objective ($f = 2$ mm) of NA $= 0.9$ on the sample on a PI P-611.3 NanoCube XYZ $100 \times 100 \times 100$ μm closed loop piezo-driven stage. The reflected beam is split by the polarizing beam splitter and mirrors into two beams of orthogonal linear polarizations recorded on the same CCD camera.

In the experimental setup, the intensity data captured in the camera simultaneously provide information for x and y directions by monitoring the difference in energy between two lobes. The left-right (LR) signal, obtained from the x-polarized field, is shown in the left column of Figs. 3(a) and 3(c), while the top-bottom (TB) signal, obtained from the y-polarized field, is shown in the right column of Figs. 3(b) and 3(d). The top row [Figs. 3(a) and 3(b)] is for full aperture illumination, and the bottom row is for annular aperture $0.5 \leq \mathrm{NA} \leq 0.9$. The annular aperture, created by using the SLM to shape the pupil, is known to enhance the longitudinal field generation for radial polarization [16], and so it should be more effective in detection. This is seen in Fig. 3, where the bottom row has a larger size of the "patch" in the particle location, implying it has been detected from a larger distance. This is useful to reduce the number of scan lines for faster detection.

To localize the particle, it is necessary to find the zero-crossing positions, which translates to finding the minimum between the two peaks when absolute values are plotted.

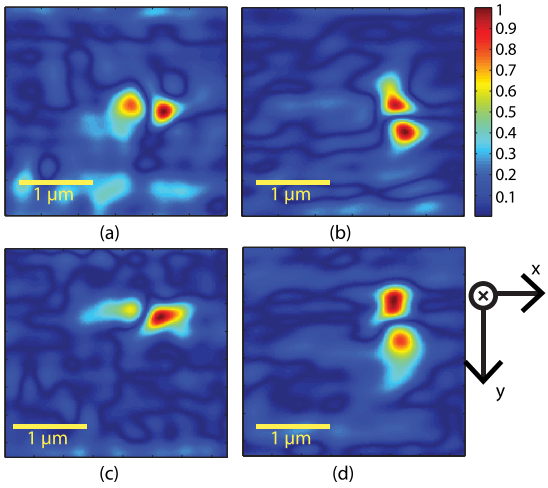

FIG. 3 (color online). Experimental LR and TB differential scanning maps of a 3×3 μm^2 area of the sample containing one nanoparticle. A Gaussian low-pass filter has been applied to reduce noise of the data. The plots are normalized and in absolute numbers. To draw the maps, first, frames on the rightmost line parallel to y are taken as a reference. Each of them is subtracted from all other frames on the same scan line parallel to x to eliminate effects of internal reflections from optical elements. Then, differential signals are calculated between TB or LR halves (for example, $LR = \left| \iint_L |E_x^{\mathrm{pupil}}|^2 - \iint_R |E_x^{\mathrm{pupil}}|^2 \right|$, where L and R, respectively, denote the left and right half of the pupil). Finally this signal is normalized by the maximum of each map. (a) LR : FULL PUPIL, (b) TB : FULL PUPIL, (c) LR : ANNULAR PUPIL, and (d) TB : ANNULAR PUPIL.

This is a different numerical problem than image-based localizations [22,23]. The final convergence will be determined by the sensitivity of the method which is dependent mainly on the slope of the signal and the measurement noise level. A closer look at the slope is shown in Fig. 4. In the top of Fig. 4, the experimental LR cross section is shown for both the full and annular apertures, parallel to x. A positive detection is made when the SNR reaches above a certain threshold. Thus, detection is more effective with the annular aperture, for which we have an approximately 20% wider signal. This also proves that the dipoles excited by longitudinal components are contributing more to the signal than transverse ones. The slope near the minimum is almost similar for both cases, because, when the particle approaches very close to the center of the spot, relative amplitudes of longitudinal to transverse components become almost similar for both apertures. In the bottom of Fig. 4, LR and TB signals are plotted for the same scan line parallel to y. The scanning direction is also reflected by the number of peaks in each signal. Specifically, a changing sign of TB signal, which is evident from the two peaks, indicates that the scanning direction is y. This is an important reason for independent localization in two orthogonal directions and, therefore, the working of this method. Near the spot center, the slope seen in the measured signal is about 0.75%/nm for TB and 0.65%/nm for LR (fraction of the maximum signal), somewhat smaller than the slope predicted from the theory (Fig. 1). For the present experiment, since no special noise control was used, the noise values were typically higher (4% and 6% of maximum signal, in TB and LR, respectively, indicated approximately by the black arrow), yielding a positional uncertainty $\Delta x \Delta y \approx (\text{noise/slope}) \approx 7.7 \times 3\ \text{nm}^2$. This is on the same order of accuracy as obtained by tracking of individual fluorescent molecules [24]. Special noise controls can reduce the noise significantly; for example, a noise level of 1% of the maximum signal can yield $\Delta x \Delta y \approx 2 \times 2\ \text{nm}^2$ using this method.

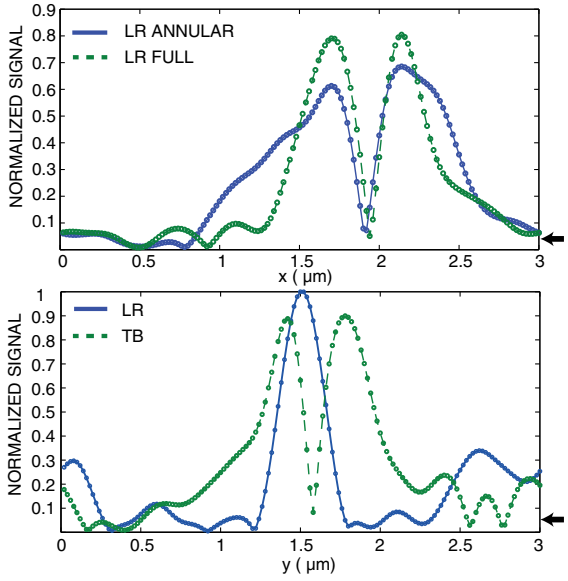

FIG. 4 (color online). Top: Experimental LR profile comparison along x for the annular aperture (blue solid line) and full aperture (green broken line). Bottom: Experimental LR (blue solid line) and TB (green broken line) profile of the same scan line parallel to y. For both figures, the experimental noise level is shown by the black arrow, approximately to scale. Actual scan points are spaced 20 nm apart.

In conclusion, we present a fast detection and localization method of an isolated subwavelength scatterer using radially polarized light and a differential detection scheme. Although a camera and an piezo scanner are used in primary experimental verification of the principle, in a production environment commercial actuators and a pair of differential detectors (similar to Ref. [2]) can be used to obtain a detection speed on the order of centimeters per second and a detection-localization speed of tens of millimeters per second, like compact-disk readers [25]. Our final results show that a localization accuracy of $\approx 10^{-4}\lambda^2$ is possible with a particle of area $\approx(\lambda^2/16)$, almost independently in two orthogonal directions. Some ways to improve this method can be mentioned here. First, extending the benefits of pupil shaping, the illumination can be even better optimized for the specific problem parameters [26]. Second, the substrate can also be modeled to enhance the interaction [27] (if it is possible to be chosen). Third, for these results, we have taken the final scan line parallel to y as a reference. In principle, the reference position can be anywhere, chosen randomly or systematically, provided it is sufficiently far from the scatterer. In this way, under a noisy environment, it is possible to take several measurements from a single experiment and average the results. Finally, this method can also be used to determine the direction of motion of a moving scattering particle under a stationary spot by rotating the polarizing beam splitter such that either the LR or the TB signal attains minimum modulation, which will then show the direction orthogonal to the particle motion.

The authors acknowledge Dr. Gopika KP Ramanandan of Delft University of Technology for performing particle size measurements with scanning electron microscope and Christiaan Hollemans of Netherlands Organisation for Applied Scientific Research (TNO), Delft for providing the sample. This research was supported by the Seventh Framework Program (FP7/2007–2013 of the European Union) under Grant Agreement No. 281027.

*S.Roy@tudelft.nl

[1] T. Plakhotnik and V. Palm, Phys. Rev. Lett. **87**, 183602 (2001).

[2] A. Mitra, B. Deutsch, F. Ignatovich, C. Dykes, and L. Novotny, ACS Nano **4**, 1305 (2010).
[3] Editorial, Nat. Photonics **3**, 361 (2009).
[4] R. R. Søndergaard, M. Hösel, and F. C. Krebs, J. Polym. Sci. B **51**, 16 (2013).
[5] F. C. Krebs, T. Tromholt, and M. Jørgensen, Nanoscale **2**, 873 (2010).
[6] H. Rooms, J. Tripathi, M. Coenen, and P. Groen, in *Proceedings of the 10th International Conference on Coatings on Glass and Plastics, Dresden*, Germany, 2014 (to be published).
[7] A. J. Oostra, P. W. Blom, and J. J. Michels, Org. Electron. **15**, 1166 (2014).
[8] A. Okamoto, H. Kuniyasu, and T. Hattori, IEEE Trans. Semicond. Manuf. **19**, 372 (2006).
[9] J. van der Donck, R. Snel, J. Stortelder, A. Abutan, S. Oostrom, S. van Reek, B. van der Zwan, and P. van der Walle, Proc. SPIE Int. Soc. Opt. Eng. **7969**, 79691S (2011).
[10] J. Pospíšil and S. Nešpurek, Prog. Polym. Sci. **25**, 1261 (2000).
[11] B. Deutsch, R. Beams, and L. Novotny, Appl. Opt. **49**, 4921 (2010).
[12] O. G. Rodríguez-Herrera, D. Lara, K. Y. Bliokh, E. A. Ostrovskaya, and C. Dainty, Phys. Rev. Lett. **104**, 253601 (2010).
[13] L. Novotny and B. Hecht, in 1st ed. *Principles of Nano-Optics* (Cambridge University Press, Cambridge, 2006), pp. 484–486.
[14] J. Braat, S. van Haver, A. Janssen, and P. Dirksen, in *Progress in Optics*, Vol. 51, edited by E. Wolf (Elsevier, Amsterdam, 2010), Chap. 6, pp. 349–468.
[15] Reference [13], pp. 56–60.
[16] R. Dorn, S. Quabis, and G. Leuchs, Phys. Rev. Lett. **91**, 233901 (2003).
[17] Q. Zhan and J. Leger, Opt. Express **10**, 324 (2002).
[18] X. Wei, A. J. Wachters, and H. P. Urbach, J. Opt. Soc. Am. A **24**, 866 (2007).
[19] C. Teichert, J. F. MacKay, D. E. Savage, M. G. Lagally, M. Brohl, and P. Wagner, Appl. Phys. Lett. **66**, 2346 (1995).
[20] Q. Zhan, Adv. Opt. Photonics **1**, 1 (2009).
[21] H. Wang, L. Shi, B. Lukyanchuk, C. Sheppard, and C. T. Chong, Nat. Photonics **2**, 501 (2008).
[22] N. Bobroff, Rev. Sci. Instrum. **57**, 1152 (1986).
[23] Reference [13], pp. 111–121.
[24] A. Yildiz, J. N. Forkey, S. A. McKinney, T. Ha, Y. E. Goldman, and P. R. Selvin, Science **300**, 2061 (2003).
[25] G. Bouwhuis, J. Braat, A. Huijser, J. Pasman, G. van Rosmalen, and K. Schouhamer-Immink, in *Principles of Optical Disc Systems* (Adam Hilger, Bristol, 1985), pp. 70–71.
[26] H. P. Urbach and S. F. Pereira, Phys. Rev. Lett. **100**, 123904 (2008).
[27] Y. Hennequin, C. P. Allier, E. McLeod, O. Mudanyali, D. Migliozzi, A. Ozcan, and J.-M. Dinten, ACS Nano **7**, 7601 (2013).